A compact T-branch beam splitter based on anomalous reflection in two-dimensional photonic crystals

Yifeng Shen (沈义峰)[1,3], Jian Sun (孙 建)[1], Xiaopeng Shen (沈晓鹏)[1], Juan Wang (王 娟)[1], Lulu Sun (孙露露)[1], Kui Han (韩 奎)[1], and Guozhong Wang (王国中)[2,3]

[1]*Department of Physics, China University of Mining and Technology, Xuzhou 221008*

[2]*School of Physics and telecommunication, Wenzhou University, Wenzhou 325035*

[3]*State Key Laboratory of Functional Materials for Informatics, Shanghai Institute of Microsystem and Information Technology, Chinese Academy of Sciences, Shanghai 200050*

Received March 13, 2008

We project a compact T-branch beam splitter with a micron scale using a two-dimensional (2D) photonic crystal (PC). For TE polarization, one light beam can be split into two sub-beams along opposite directions. The propagating directions of the two splitting beams remain unchanged when the incident angle varies in a certain range. Coupled-mode theory is used to analyze the truncating interface structure in order to investigate the energy loss of the splitter. Simulation results and theoretical analysis show that choosing an appropriate location of the truncating interface (PC-air interface) is very important for obtaining high efficiency due to the effect of defect modes. The most advantage of this kind of beam splitter is being fabricated and integrated easily.

OCIS codes: 230.1360, 120.1680.

doi: 10.3788/COL20080610.0709.

Since its inception, photonic crystal (PC) has attracted much interest due to its ability to control the flow of light[1,2]. In recent years, there have been lots of researches on self-collimation effect[3−14], which means a beam of electromagnetic wave can propagate with almost no diffraction in a perfectly periodic PC. When a self-collimated beam propagating in a PC incidents upon the interface between the PC and a homogeneous dielectric (i.e., air), it will be reflected and the direction of the reflected beam is almost independent of the orientation of the interface (namely, the reflected beam's direction has little business with the incident angle in a certain range). This phenomenon is called anomalous reflection. Yu *et al.* designed a beam bend device using this effect[13]. But they did not consider the localized light scattering of the defect air-holes at the truncating surface. These defect modes may be strong enough to lead heavy energy loss especially for large incident angles. Recently Chen *et al.* have given a study on the line defect mode by coupled-mode theory[14]. But they did not consider the case for defect modes caused by surface truncation.

In this letter, using a two-dimensional (2D) PC, we propose a micron scale T-branch beam splitter based on anomalous reflection effect. For TE polarization (TE polarization has a magnetic field **H** parallel to the axis of the air holes), one beam can be separated into two branches along opposite directions[15]. The magnetic-field distribution was simulated by the finite-difference time-domain (FDTD) method[16]. In addition, we investigate the effect on the intensity of the two sub-beams for different shapes and locations of the beam splitter. Simulation results show that choosing an appropriate location of the truncating interface (PC-air interface) is very important to obtain a high reflection due to the effect of defect modes. Detailed analyses for defect modes are considered. The well-known coupled-mode theory is used to analyze the truncating interface structure by considering the coupling between the self-collimated modes and the surface defect modes.

Reference [12] introduced a PC structure which consists of a square lattice of air holes introduced into silicon material (with a refractive index $n = \sqrt{12}$). This PC structure has a good self-collimation character along Γ-M direction in the frequency range from 0.186 to $0.192c/a$, where c and a represent the light velocity and lattice constant, respectively. In the context, we also adopt this PC structure and keep the work frequency $f = 0.190c/a$ in the FDTD simulation. The PC structure consists of a $18\sqrt{2}a \times 45\sqrt{2}a$ square lattice of air holes introduced into a high index material Si ($n = \sqrt{12}$) and the holes have a radius of $0.35a$, where n is the dielectric index. A 2D X-Y orthogonal coordinate system is established as shown in Fig. 1, whose origin locates at the center of one air hole. Obviously, the X-direction is along the Γ-M direction. We introduce a triangular air area (the white isosceles triangle region in Fig. 1), which behaves as a beam splitter, into the PC structure. Parameters of the isosceles triangle are set as follows: the vertex is $(-0.6a, 0)$, the vertex angle is defined as 2θ, where θ is in a range from 35° to 45°, and the height is set as a constant of $10a$ for the convenience of discussion. The device can be easily realized by etching away the triangular Si-air holes area in the fabrication process.

In the structure of Fig. 1, a continuous Gaussian type source (the black cross) with a $6a$ width is placed at $(-16.5a, 0)$ and the work frequency is set as $0.190c/a$. The light beam propagates along the Γ-M direction keeping a self-collimating character. In the context we only consider the TE polarization. Three power monitors (marked as I, II, III) are introduced into the PC structure, which are located at $(-8.5a, 0)$, $(1.5a, 19a)$,

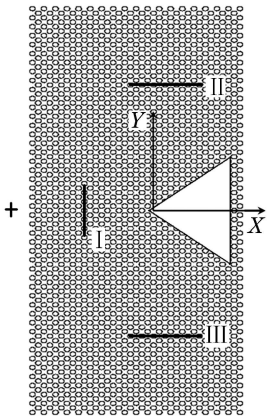

Fig. 1. Sketch map of the beam splitter. The white triangle area represents the splitter, the black broad lines (I, II, and III) are power monitors, and the black cross indicates a light source with a Gaussian shape.

and $(1.5a, -19a)$, respectively. All these monitors are identical with a width of $7\sqrt{2}a$, which is larger than the beam width of $6a$ so that most of the energy can be collected by these monitors. Perfect matching layer (PML) boundary condition is used here[17]. And we can get the magnetic field distributions for different conditions by FDTD simulations.

For the first condition we locate the source at $(-16.5a, 0)$ and the vertex of the triangular air area at $(-0.6a, 0)$, and change the vertex angle of the splitter. We simulate the field distributions at different angles. Figures 2(a) and (b) show the field maps for $\theta = 45°$ and $\theta = 35°$, respectively. The incident angle is equal to $90° - \theta$ as the beam incidents along the Γ-M direction.

From Fig. 2(a), the incident angle is 45° and the reflection is a normal reflection which satisfies the Snell's law. One incident beam is split into two separated sub-beams by the splitter device and one sub-beam propagates along the positive Y-direction, while the other propagates along the negative Y-direction. But in Fig. 2(b) the incident angle is 55° and the reflection does not satisfy the Snell's law, which is corresponding to an anomalous reflection. Under this condition, the two separated sub-beams still keep collimation along the positive Y-direction and negative Y-direction with almost the same beam width as that of the incident beam. To evaluate the maximum range of the incident angle, with which the reflected beams still keep the same directions, we simulate the field maps for different angles of 2θ from 64° to 94° with a step of 2°. The power of each separated beam can be obtained by power monitors II and III and can be normalized with respect to the incident beam's power from the monitor I. In the following discussions, we always use this normalized intensity values. Considering the symmetry, the power of each separated sub-beam is identical. So the power of the whole outgoing beams (the two separated sub-beams) is double of each beam's power. Figure 3(a) gives the normalized intensity of the whole output beams as a function of the parameter 2θ.

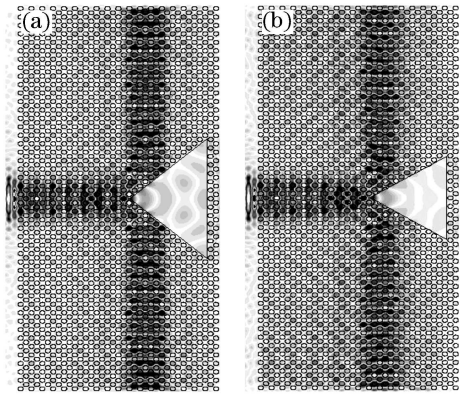

Fig. 2. Steady-field patterns of FDTD simulation for the case of (a) $\theta = 45°$ and (b) $\theta = 35°$. The vertex angle of the splitter is defined as 2θ.

Seen from Fig. 3(a), there is an angle range between 70° and 90°, in which the normalized intensity of the whole output beams keeps a high value above 0.8 implying a good self-collimation effect. This phenomenon can be explained using the equal frequency contour (EFC) analysis. Figure 3(b) gives the EFC of the PC at the working frequency $f = 0.190c/a$ for the TE polarization. The EFC has a square shape around the M point and each side of the square has a linear part in the Brillouin zone. It is known that the light propagation direction in PC is identical to the direction of group velocity given by $\vec{v}_{\rm g} = \nabla_k \omega(\vec{k})$, where ω and $\vec{k}$ are the optical frequency and wave vector, respectively. The reflected beam will be fixed on the Γ-M direction in spite of small variety of the direction along which the interface is truncated if the $\vec{k}$-conservation line (determined by the interface and the wave vector $\vec{k}$) crosses the EFC of the PC at the

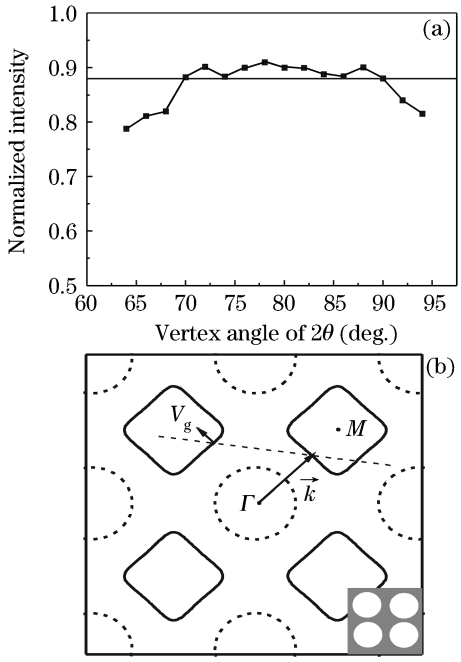

Fig. 3. (a) Normalized intensity of the whole output sub-beams varies with different vertex angles 2θ when the vertex of the splitter is located at $(-0.6a, 0)$. The horizontal line indicates normalized intensity of 0.88; (b) EFC of the PC and air at the working frequency $f = 0.190c/a$ for the TE polarization. The dashed circles represent EFC of air and the solid squares represent EFC of the PC. The dashed line is the $\vec{k}$ conversation line. The inset indicates the PC structure.

linear side of the square in the first Brillouin zone. That is the origin of anomalous reflection. On the other hand, the $\vec{k}$-conservation line does not interact with the EFC of air in the first Brillouin zone, which is corresponding to the total internal reflection. That is the reason why this splitter has so high power transmitting efficiency. The characteristic of anomalous reflection for our splitter gives a large fabrication tolerance in the sample design. This is the most advantage of our beam splitter compared with conventional splitters.

Now we take account of the location of the splitter. Fix the splitter with a shape of a right-angle isosceles triangle unchanged, that means the incident angle is kept at 45°, and translate this splitter along the X-direction. We scan the normalized intensity of the whole output beams when the vertex of the splitter translates from $-0.8a$ to $+1.5a$ on the x axis. The power monitors II and III are also removed synchronously. Figure 4 gives the curve of the normalized intensity of the whole output sub-beams varying with the X-coordinate of the splitter vertex. One can see that the curve has a flat region in the range $-0.6a < x < -0.4a$, in which the normalized intensity remains higher than 0.91. The curve has a periodic character which is corresponding to the translation period of $\sqrt{2}a$ along the x-direction. The flat region in the range $-0.6a < x < -0.4a$ reduces the request for the fabrication precision, which makes device fabrication very easy. Therefore, our design is much better than other beam splitters for a larger fabrication tolerance.

Between the two flat regions, there is a valley in the curve. The normalized intensity decreases from $-0.4a$ to $0.4a$ and then increases from $0.5a$ to $1.0a$. This phenomenon can be explained by analyzes for defect modes. When the vertex of the splitter is at the region from $-0.4a$ to $0.4a$, the silicon-air interface just cuts across into a row of air holes and these air holes are not perfect circular holes any more. So there is a row of defect air holes at the silicon-air interface. These defect air holes will scatter the incident beams and produce some localized defect modes, which will reduce the reflection. To calculate the dispersion properties of the defect modes, we use the plane wave expansion with supercell technique. The supercell is chosen with the 11 periods width and 1 period length shown in Fig. 5(a). Figure 5(a) shows the projection band diagram along the Γ-X direction for the vertex of the splitter with a coordinate $x = 0$. The gray domains on the band diagram represent the continuum of the guide modes in the bands and the solid line

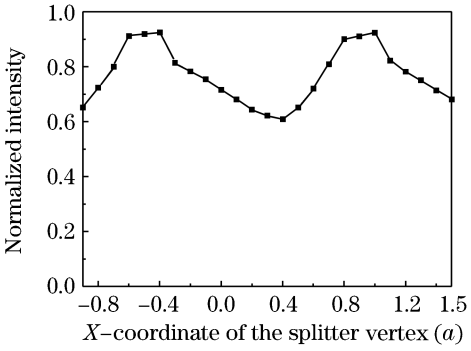

Fig. 4. Normalized intensity of the whole output beams versus the X-coordinate of the splitter vertex.

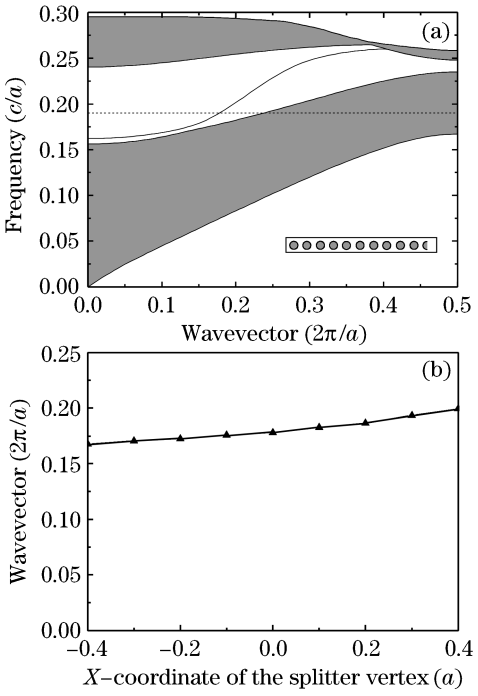

Fig. 5. (a) Projection band diagram along the Γ-X direction for the vertex of the splitter with a coordinate $x = 0$. The gray regions represent the continuum of extended modes, and the solid line represents the dispersion relation of defect modes. The dotted line represents the work frequency $f = 0.190c/a$. The inset shows the supercell structure; (b) $\vec{k}$-vector of defect modes versus the X-coordinate of the splitter vertex for the frequency of $0.190c/a$.

represents the dispersion of defect modes. Obviously, this curve has a positive slope and crosses with the dashed line (indicating the frequency $f = 0.190c/a$) at a wave vector $\vec{k} = 0.178(2\pi/a)$. The projected $\vec{k}$-vector of the self-collimated modes onto the Γ-X direction is $0.34(2\pi/a)$ for the frequency $0.190c/a$. According to the couple mode theory[18], the power-exchanged ratio is closely concerned with the difference of $\vec{k}$-vectors of two modes. The coupling efficiency increases as the mismatch between the $\vec{k}$-vectors of the self-collimated modes and the defect modes decreases. Because the defect modes mean the energy loss of the splitter, the normalized intensity of the whole output beams will decrease if the mismatch between the two $\vec{k}$-vectors becomes small. Figure 5(b) gives the relation curve between the $\vec{k}$-vector of the defect modes and the X-coordinate of the splitter vertex. It is shown that, when the X-coordinate of the splitter vertex increases in the range from $-0.4a$ to $0.4a$, the $\vec{k}$-vector of the defect modes increases and becomes more and more close to the projected $\vec{k}$-vector of self-collimated mode. So the couple efficiency is increasing while the energy loss of the splitter becomes larger and larger. This is just the reason why the normalized intensity of the whole output beams decreases in the range of $-0.4a < x < 0.4a$.

When the vertex of the splitter is at the region from $0.5a$ to $1.0a$, the silicon-air interface does not cut with any rows of air holes. So the interface between the air-splitter area and the PC structure is a perfect plane, and there is a silicon cladding between the perfect photonic

crystal and the air splitter at this condition. Reference [19] has mentioned that leaky modes will be depressed as the cladding thickness increases which leads to high reflection. So the increase of reflection is due to two factors: one is the vanishing of defect modes and the other is the depression of leaky modes.

FDTD simulations and analysis show two characters of our design: 1) The propagating direction of the two separated-beam is pinned along the vertical direction and the reflected beams keep a high intensity if the vertex angle of the beam splitter varies among the range of 20 degrees from 70° to 90°; 2) When the X-coordinate of the splitter vertex is among the range from $-0.6a$ to $-0.4a$ (the Y-coordinates are all zero), the whole power of the two output sub-beams reaches over 0.91 (normalized by incident beam power). In other words, these advantages allow us to make certain errors in practical implement, and reduce the request for the fabrication precision. Our projected beam splitter is based on anomalous reflection effect at self-collimation frequencies, so in general, it can be split into two parts by a triangle-shape-splitter for a collimation beam. For the working wave length of 1.55 μm in optical communication, parameters can be chosen as bellow: the lattice constant $a = 294.5$ nm, the radii of the air holes $r = 103$ nm, and the height of the triangle $h = 1030.8$ nm. Compared with conventional splitters, which are hardly integrated with mirrors or prisms to split an incoming light beam, this kind of T-branch beam splitter has two novel characters: one is having a large tolerance for fabrication, synchronously keeping a high intensity for reflected beams, the other is having an ultra-compact size. Our splitter is only micron scale. These characters make it a candidate in optical integrated circuits.

The work was supported by the Science Foundation of China University of Mining and Technology under Grant No. OK061065. Y. Shen's e-mail address is shen_syf@163.com.

References

1. E. Yablonovich, Phys. Rev. Lett. **58,** 2059 (1987).
2. S. John, Phys. Rev. Lett. **58,** 2486 (1987).
3. J. W. Hans, M. Siraj, P. Prasad, and P. Markowicz, Chin. Opt. Lett. **5,** 527 (2007).
4. X. Shen, K. Han, X. Yang, Y. Shen, H. Li, G. Tang, and Z. Guo, Chin. Opt. Lett. **5,** 662 (2007).
5. H. Kosaka, T. Kawashima, A. Tomita, M. Notomi, T. Tamamura, T. Sato, and S. Kawakami, Appl. Phys. Lett. **74,** 1212 (1999).
6. J. Witzens, M. Loncar, and A. Scherer, IEEE J. Sel. Top. Quantum Electron. **8,** 1246 (2002).
7. D. N. Chigrin, S. Enoch, C. M. S. Torres, and G. Tayeb, Opt. Express **11,** 1203 (2003).
8. L. Wu, M. Mazilu, and T. F. Krauss, J. Lightwave Technol. **21,** 561 (2003).
9. C. H. Chen, A. Sharkawy, D. M. Pustai, S. Y. Shi, and D. W. Prather, Opt. Express **11,** 3153 (2003).
10. D. W. Prather, S. Y. Shi, D. M. Pustai, C. H. Chen, S. Venkataraman, A. Sharkawy, G. J. Schneider, and J. Murakowski, Opt. Lett. **29,** 50 (2004).
11. D. M. Pustai, S. Y. Shi, C. H. Chen, A. Sharkawy, and D. W. Prather, Opt. Express **12,** 1823 (2004).
12. X. F. Yu and S. H. Fan, Appl. Phys. Lett. **83,** 3251 (2003).
13. X. F. Yu and S. H. Fan, Phys. Rev. E **70,** 055601 (2004).
14. H. B. Chen, Z. F. Li, W. Liu, F. H. Yang, S. L. Feng, and H. Z. Zheng, Opt. Commun. **262,** 120 (2006).
15. J. D. Joannopoulous, S. G. Johnson, J. N. Winn, and R. D. Meade, *Photonic Crystals:Molding the Flow of Light* 2nd edn. (Princeton University Press, Princeton, New Jersey, 2008) p67.
16. A. Taflove, *Computational Electrodynamics: The Finite-Difference Time-Domain Method* (Artech House, Boston, 1995) p36.
17. R. G. Hunsperger, *Integrated Optics: Theory and Technology* (Springer, Tokyo, 1995).
18. S. L. Chuang, IEEE J. Quantum Electron. **23,** 499 (1987).
19. J. L. He, J. Yi, and S. L. He, Opt. Express **14,** 3024 (2006).